THE JOURNAL OF PHYSICAL CHEMISTRY C

Subscriber access provided by UNIV OF SCIENCES PHILADELPHIA

C: Surfaces, Interfaces, Porous Materials, and Catalysis

A Comparative *Ab Initio* Study of Anhydrous Dehydrogenation of Linear-Chain Alcohols on Cu(110)

Wei Chen, Ekin Dogus Cubuk, Matthew M. Montemore, Christian Reece, Robert J. Madix, Cynthia M. Friend, and Efthimios Kaxiras

J. Phys. Chem. C, **Just Accepted Manuscript** • DOI: 10.1021/acs.jpcc.8b01698 • Publication Date (Web): 27 Mar 2018

Downloaded from http://pubs.acs.org on March 28, 2018

Just Accepted

"Just Accepted" manuscripts have been peer-reviewed and accepted for publication. They are posted online prior to technical editing, formatting for publication and author proofing. The American Chemical Society provides "Just Accepted" as a service to the research community to expedite the dissemination of scientific material as soon as possible after acceptance. "Just Accepted" manuscripts appear in full in PDF format accompanied by an HTML abstract. "Just Accepted" manuscripts have been fully peer reviewed, but should not be considered the official version of record. They are citable by the Digital Object Identifier (DOI®). "Just Accepted" is an optional service offered to authors. Therefore, the "Just Accepted" Web site may not include all articles that will be published in the journal. After a manuscript is technically edited and formatted, it will be removed from the "Just Accepted" Web site and published as an ASAP article. Note that technical editing may introduce minor changes to the manuscript text and/or graphics which could affect content, and all legal disclaimers and ethical guidelines that apply to the journal pertain. ACS cannot be held responsible for errors or consequences arising from the use of information contained in these "Just Accepted" manuscripts.

ACS Publications

is published by the American Chemical Society. 1155 Sixteenth Street N.W., Washington, DC 20036

Published by American Chemical Society. Copyright © American Chemical Society. However, no copyright claim is made to original U.S. Government works, or works produced by employees of any Commonwealth realm Crown government in the course of their duties.

A Comparative *Ab Initio* Study of Anhydrous Dehydrogenation of Linear-Chain Alcohols on Cu(110)

Wei Chen,[†,‡] Ekin Dogus Cubuk,[†,‡] Matthew M. Montemore,[¶,‡] Christian Reece,[¶] Robert J. Madix,[*,¶,‡] Cynthia M. Friend,[¶,‡] and Efthimios Kaxiras[*,†,‡]

†*Department of Physics, Harvard University, Cambridge, MA 02138, USA*

‡*John A. Paulson School of Engineering and Applied Science, Harvard University, Cambridge, MA 02138, USA*

¶*Department of Chemistry and Chemical Biology, Harvard University, Cambridge, MA 02138, USA*

E-mail: rmadix@seas.harvard.edu; kaxiras@physics.harvard.edu

Abstract

The catalytic behavior of Cu surfaces in the anhydrous production of aldehydes from alcohols, a process of industrial significance, is puzzling: the two simplest alcohols (methanol and ethanol) show dramatically different decomposition behavior on Cu. Here, we study the thermodynamic and kinetic processes involved in the anhydrous dehydrogenation of linear-chain alcohols including methanol, ethanol, 1-propanol, and 1-butanol on the Cu(110) surface using multiscale approaches. First, we obtain the adsorption structures and energies of the reaction intermediates, in which van der Waals (vdW) interactions play a crucial role. Then we determine the kinetic barriers for the two dehydrogenation steps, namely the O–H and the subsequent C–H bond breaking on Cu. The reaction of methoxy to formaldehyde has a rather high energy transition state, in contrast to that of alkoxide to aldehyde in the longer chain systems. This difference qualitatively explains the lower production efficiency of formaldehyde on Cu. Finally, we simulate the production rates of aldehydes based on which we optimize reaction conditions and propose possible avenues for enhancing the production of anhydrous formaldehyde using Cu-based catalysts.

Introduction

Aldehydes, especially formaldehyde (CH_2O), with millions of tons produced per year, are key precursors to many important chemical compounds. Currently, formaldehyde is manufactured by oxidative dehydrogenation of methanol (CH_3OH) using silver-based catalysts, with water as a byproduct: $2\ CH_3OH + O_2 \rightarrow 2\ CH_2O + 2\ H_2O$.[1–8] It is desirable to dehydrogenate methanol to formaldehyde anhydrously, $CH_3OH \rightarrow CH_2O + H_2$, that is, without production of water, at moderate temperatures over non-precious metals, such as Cu or Ni so that the high energy-cost process of formaldehyde/water separation can be eliminated,[9–15] with the H_2 byproduct being useful as a clean fuel. Copper catalyzes anhydrous acetaldehyde (CH_3CHO) production from ethanol (CH_3CH_2OH) at around 200-300 °C,[16–19] while

the production of formaldehyde from methanol requires either the addition of a promoter (pre-adsorption of oxygen or water) or extremely high reaction temperatures.[2,10,12,20] Given that methanol and ethanol, which differ by only one carbon atom in the carbon skeleton, are the two simplest alcohols, it is important to explain the mechanisms responsible for their very different dehydrogenation behavior over Cu. Insights into this important issue may lead to more efficient formaldehyde production.

We focus here on the Cu(110) surface because of the lower coordination numbers of the top-row atoms, which imply that this surface of Cu may be more reactive than the (111) and (100) surfaces[21–23] for methanol decomposition. Several theoretical studies have been performed on the dehydrogenation of methanol[13,15,24–29] and ethanol[30–33] on Cu. For example, Mei *et al.*[25] mapped out the potential energy surface of methanol decomposition on Cu(110). However, no studies have yet included van der Waals (vdW) interactions to explore the reaction mechanisms on Cu(110). An increasing number of theoretical investigations[34–44] have demonstrated that vdW corrections are critical in order to accurately characterize the reactivity and selectivity in surface catalysis. Extending these investigations to longer chain alcohols, such as 1-propanol and 1-butanol, can lead to a deeper understanding of how dehydrogenation behavior scales with respect to the carbon chain length.

In this paper, we compare the thermodynamic and kinetic processes in the anhydrous dehydrogenation of four different alcohols on Cu(110) using multiscale approaches, combining first-principles calculations and microkinetic rate analysis. First, we calculate the adsorption structures and energies of the reaction intermediates on the surface, with the inclusion of vdW interactions. Next, we determine the kinetic barriers of alcohol decomposition on Cu. We find that methanol exhibits different kinetic pathways from the other alcohols. We simulate the production rates of aldehydes on Cu(110), and based on these results we propose possible approaches to enhance the production of anhydrous formaldehyde using Cu-based catalysts.

Methods

Our density functional theory (DFT) calculations were performed using the Vienna *ab initio* simulation package (VASP),[45] with the projector-augmented wave (PAW) potentials.[46,47] The generalized gradient approximation parameterized by Perdew-Burke-Ernzerhof (GGA-PBE)[48] was employed for the exchange-correlation functional. GGA functionals generally provide improved results over the local density approximation (LDA) functional because the former depends not only on the local charge density, but also on the spatial variation of the density. The energy cutoff was 400 eV for the plane-wave basis sets. The method developed by Tkatchenko and Scheffler[49] was used to account for the vdW interactions. The lattice constant of Cu was obtained via structural optimization. The Cu(110) surfaces were modeled by slabs of four-atomic-layer-thick 3×4 supercell. The vacuum region was longer than 10 Å to ensure decoupling between neighboring images. During relaxation, the bottom-layer Cu atoms were fixed in their respective bulk positions, and all the other atoms, including the adsorbates, were fully relaxed until the force on each atom was smaller in magnitude than 0.01 eV/Å. A Γ-centered $5\times5\times1$ k-point mesh was utilized for the 3×4 supercell.[50] The supercell size is large enough so that the inter-molecule vdW interactions are ignored in the calculations. This corresponds to experiments with low coverages of surface intermediates. The climbing image nudged elastic band (CI-NEB) method,[51] with five to eleven intermediate images constructed along each pathway, and the Dimer method,[52] were both used to determine the potential energy barriers of various reaction processes. We used the NEB method to find the rough structure of the transition state, followed by the Dimer method to find the accurate one. Then the NEB method was used again to confirm that the reaction path is complete without including other higher-energy transition states. Although the DFT calculation often includes absolute errors in the estimation of adsorption energies and kinetic barriers, it performs much better for comparing the energetics across similar systems because of cancellation of systematic errors.

Results and Discussion

Thermodynamics: adsorption configurations and energies

First, we optimized the adsorption structures of various reaction intermediates during the dehydrogenation of alcohols on Cu(110). After obtaining the most stable configurations, we calculated the adsorption energies (E_{ads}) of each adsorbate using DFT total energies (Table 1): E_{ads}=$E_{\mathrm{ads/Cu}}$−E_{gas}−E_{Cu}, where $E_{\mathrm{ads/Cu}}$ is the total energy of the Cu surface with an adsorbed molecule, E_{gas} is the energy of the gas-phase adsorbate, and E_{Cu} is the energy of the bare Cu(110) surface. With this definition, E_{ads} measures the energy required for each adsorbate to desorb from the surface to the gas phase.

The E_{ads} values without vdW corrections of different alcohols are roughly the same, as are the values for different alkoxides. Among aldehydes, since CH_2O is the most reactive, its E_{ads}, relating to its chemical bonding to the surface, is the strongest. The vdW interactions contribute significantly to the overall E_{ads}. Specifically, the vdW-enhanced E_{ads} has an approximately linear dependence on the carbon chain length of the adsorbate, with an increase of about 0.1-0.2 eV per CH_2 group.

The vdW corrections are indeed necessary for predicting the stability of adsorbates on the Cu(110) surface (Table 1). The E_{ads} of methanol on Cu(110) was estimated experimentally to be −0.70 eV from temperature-programmed desorption (TPD) measurements.[2] Without including the vdW correction, our result is −0.39 eV and previous studies using different functionals predicted −0.34 eV, −0.41 eV, and −0.55 eV.[24,25,53] Here the DFT-TS method reasonably reproduces the experimental E_{ads} value, to within 0.04 eV, yielding a value of −0.74 eV. We tested vdW-DF2,[54–56] a different vdW correction, and found $E_{\mathrm{ads}} = -0.45$ eV for methanol. Thus, the DFT-TS correction yields a better description of the interaction between methanol and Cu than the vdW-DF2 correction. Our displacement experiments[57] indicate that ethoxy is more stably adsorbed on the Cu(110) surface than methoxy. This trend is only reproduced when vdW interactions are included (Table 1). Calculations without

vdW predict that methoxy and ethoxy have almost the same E_{ads}, while the results with vdW give stronger adsorption of ethoxy on Cu than that of methoxy by 0.14 eV. The following results were calculated within the framework of the vdW interactions implemented by DFT-TS.

The most stable adsorption configurations of all reaction intermediates investigated have oxygen bonded with the top-row Cu atoms, except for formaldehyde that forms both Cu–O and Cu–C bonds with the substrate (Fig. 1). All the alcohols adsorb at the Cu top sites, with the Cu–O bond tilted by 21.8° (methanol), 21.7° (ethanol), 20.2° (1-propanol), and 20.5° (1-butanol) relative to the surface normal ($\hat{\mathbf{n}}$), respectively. All the alkoxides adsorb at the short bridge sites, with a distance of ∼1.96 Å between O and the neighboring Cu atoms. At the equilibrium structure the carbon chains assume an orientation that approximately aligns with the Cu chains along the $[1\bar{1}0]$ direction (see top views in Figs. 4 and 5, discussed in the next section). Among aldehydes, formaldehyde lies between two Cu rows in a long bridge site, a configuration more stable than the others by more than 0.2 eV. Acetaldehyde adsorbs at the short bridge site with the two Cu–O bonds being slightly different in length (Table 1). The two larger aldehydes adsorb at the top sites. As compared to the gas phase, the O–C bond length is elongated when aldehyde is adsorbed on the surface. The increase in bond length differs for the aldehydes (formaldehyde: 0.17 Å, acetaldehyde: 0.03 Å, propionaldehyde and butyraldehyde: 0.02 Å) because of their varying adsorption sites. The Cu–O bond lengths of alkoxides adsorbed on Cu are smaller than those of alcohols and aldehydes (Table 1), a result that correlates well with the fact that the binding energies of alkoxides are much larger than the other adsorbates on Cu(110). The vdW interactions do not change the adsorption site and only alter slightly the bond lengths of Cu–O (except for acetaldehyde), O–C, and C–C (for adsorbates with at least two C atoms), based on a comparison of the structural parameters obtained from the PBE and PBE+vdW calculations. However, the bond angles change, due to the vdW forces that bring the adsorbate in closer contact with the substrate (Table 1). For example, the angle between the C–O bond and $\hat{\mathbf{n}}$ increases from 48.0° to 52.2°

when the vdW correction is applied to methanol adsorption on Cu.

Kinetics: O–H and C–H bond breaking barriers

The differing energetics of equilibrium structures do not provide a resolution of the different dehydrogenation behavior of methanol and ethanol on Cu. We therefore turn to the potential energy paths of the reaction steps involved in the anhydrous production of aldehydes. Starting from the stable adsorption structures, we calculated the bond-breaking barriers of O–H in the alcohols and of the β-C–H bond in the alkoxides. In Fig. 2 the gas-phase energy of each alcohol is set at $E = 0$, and the energy levels of different reaction stages are displayed accordingly. The energies of alkoxides(a) are calculated with the dissociated H atoms from the respective alcohols in the form of adsorbed atomic H. The production of formaldehyde ($CH_2O{\cdot\cdot}H(a)$) from the adsorbed state of methanol ($CH_3OH(a)$) is endothermic by 1.00 eV (0.74+0.26, Fig. 2a), larger than that of acetaldehyde formation from ethanol which is 0.65 eV (0.89−0.24, Fig. 2b). Therefore, consideration of only the reaction energies suggests that methanol dehydrogenation should be more difficult than ethanol dehydrogenation.

Similar values are observed for the O–H bond breaking barriers of the four alcohols (Fig. 2). Cleavage of the O–H bond in methanol leads to H and methoxy adsorbed in two separated short bridge sites (Fig. 3a), with a barrier of 0.71 eV. During this process $CH_3OH(a)$ (−0.74 eV) has to first rotate[25] to become $CH_3OH'(a)$ (−0.68 eV), the latter having the dissociating H closer to the short bridge position. Similarly, for ethanol decomposition, the O–H bond breaking barrier is 0.72 eV, higher by only 0.01 eV, which is a negligible difference considering the calculation accuracy. This barrier becomes 0.71 eV for 1-propanol and 0.68 eV for 1-butanol. By comparing the detailed structures, we find that the important structural parameters in the transition states (see TS1 in Fig. 3), including O–H, O–Cu, and Cu–H distances (see bar plots in Fig. 3), are essentially the same for the reactions of different alcohols, consistent with the similarity of their O–H dissociation barriers.

The dehydrogenation step of methoxy has very different barrier than the other alkoxides.

The methoxy-to-formaldehyde reaction exhibits an activation energy of 0.93 eV (see TS2 in Fig. 2a, $CH_3O(a)$ to $CH_2O{\cdot\cdot}H(a)$), which matches with experimental measurement (0.91 ± 0.01 eV)[58] very well. For ethoxy-to-acetaldehyde, the β-C–H bond scission barrier is 0.56 eV (Fig. 2b). The analogous barrier is 0.55 eV for 1-propoxy (Fig. 2c) and 0.58 eV for 1-butoxy (Fig. 2d). The fact that methoxy-to-formaldehyde has a higher barrier than the others is mainly due to the substantially different diffusion paths of the dissociating H (see structures of TS2 in Figs. 4 and 5). In particular, the dissociating H in methoxy moves toward the neighboring short bridge site along the same Cu row, while in the other alkoxides H migrates towards the short bridge site along the neighboring Cu row. There is not any stable final state if H in methoxy is removed towards the nearest bridge site along the neighboring Cu row. In the transition state of methoxy-to-formaldehyde (TS2 in Fig. 4a), oxygen binds primarily with only one substrate Cu atom rather than forming two nearly identical Cu-O bonds as seen for TS2 in the other alkoxide-to-aldehyde reactions. Further, the structural configuration of formaldehyde in the transition state deviates from its most stable geometry, resulting in a high-energy transition state and thus a higher barrier than the others.

The reverse reaction, namely the H-aldehyde recombination, has very low activation energy - 0.08 eV for $CH_2O{\cdot\cdot}H(a)$ and 0.04 eV for $CH_3CHO{\cdot\cdot}H(a)$. We therefore calculate the separation of H farther away from aldehyde and obtain energy barriers of 0.08 eV for $CH_2O{\cdot\cdot}H(a)$ to $CH_2O\cdots H(a)$ and 0.22-0.27 eV for the other aldehydes (see TS3 in Fig. 2). It suggests that H and formaldehyde tend to repel each other when they are adsorbed in the neighboring short bridge sites along the same Cu row.

A close comparison with a previous non-vdW study of methanol decomposition[25] shows that, although the vdW interactions enhance significantly the adsorption energies, the kinetic barriers of methanol dehydrogenation are changed less significantly, in part due to the fact that vdW interactions contribute not only to the initial and final state energies, but also to the transition state energy, with roughly equal contributions.

Overall, the decreased production efficiency of formaldehyde[2,10,12,20] compared to ac-

etaldehyde[16–19] on Cu can be qualitatively understood by their reaction kinetics. The critical differences in C–H bond breaking barriers between methoxy and the other alkoxides are much larger than errors in the calculations which are typically < 0.05 eV. The reaction of methoxy to formaldehyde is clearly the rate limiting process; it shows a substantially higher barrier than the back reaction from methoxy to methanol, leaving methanol and methoxy as the most abundant species on the surface and preventing the formation of formaldehyde. For ethanol, after overcoming the first dehydrogenation barrier of 0.72 eV to form the adsorbed ethoxy, the reaction can smoothly proceed towards the production of acetaldehyde. The production of propionaldehyde and butyraldehyde should be less efficient than that of acetaldehyde on Cu, because of the higher desorption energies of the produced aldehydes.

Microkinetic rate analysis

So far we have limited discussions to the energetics and kinetics from first-principles calculations. It is important to try to gain more insights on the delicate competitions between the various rate processes, and potentially define the physical conditions for enhancing anhydrous production of formaldehyde on Cu. For example, it is notable that, although the barrier for reforming ethanol from ethoxy is high and the dehydrogenation barrier from ethoxy to acetaldehyde is relatively low, the β-C–H recombination rate seems high, which is detrimental to the efficient production of acetaldehyde.

Accordingly, we performed a rate analysis[59–61] based on microkinetic models to compute the production rates of various aldehydes on Cu(110). In our simulations of continuous flow reactions, we considered the elementary steps listed in Table 2. The surface fractional coverages of the reaction intermediates at time t are denoted as $\theta_1(t)$, $\theta_2(t)$, $\theta_3(t)$, and $\theta_{\mathrm{H}}(t)$, where the subscripts 1, 2, 3, and H stand for surface alcohol(a), alkoxide(a), aldehyde(a), and H(a), respectively. θ_{tot}, the sum of the coverages of surface species, does not exceed 1 that refers to a full monolayer coverage. The cumulative amounts of desorbed alcohol(g) and aldehyde(g) per surface site are denoted as $\theta_{\mathrm{alc}(g)}(t)$ and $\theta_{\mathrm{ald}(g)}(t)$ (units: molecules/site).

As shown in the following equations, we used the reaction rates (units: molecules/site/s) of the elementary steps to keep updating the concentrations of surface intermediates and the amounts of desorbed alcohol(g) and aldehyde(g).

$$
\begin{cases}
\dfrac{d\theta_{\mathrm{alc}(g)}(t)}{dt} = A_{\mathrm{de}} e^{-E_{1r}/(k_{\mathrm{B}}T)} \theta_1, \\
\dfrac{d\theta_1(t)}{dt} = -A_{\mathrm{de}} e^{-E_{1r}/(k_{\mathrm{B}}T)} \theta_1 - A_{\mathrm{di}} e^{-E_{2f}/(k_{\mathrm{B}}T)} \theta_1 (1-\theta_{\mathrm{tot}}) + A_{\mathrm{as}} e^{-E_{2r}/(k_{\mathrm{B}}T)} \theta_2 \theta_{\mathrm{H}}, \\
\dfrac{d\theta_2(t)}{dt} = 0, \\
\dfrac{d\theta_3(t)}{dt} = A_{\mathrm{di}} e^{-E_{3f}/(k_{\mathrm{B}}T)} \theta_2 (1-\theta_{\mathrm{tot}}) - A_{\mathrm{as}} e^{-E_{3r}/(k_{\mathrm{B}}T)} \theta_3 \theta_{\mathrm{H}} - A_{\mathrm{de}} e^{-E_{4f}/(k_{\mathrm{B}}T)} \theta_3, \\
\dfrac{d\theta_{\mathrm{H}}(t)}{dt} = A_{\mathrm{di}} e^{-E_{2f}/(k_{\mathrm{B}}T)} \theta_1 (1-\theta_{\mathrm{tot}}) - A_{\mathrm{as}} e^{-E_{2r}/(k_{\mathrm{B}}T)} \theta_2 \theta_{\mathrm{H}} + A_{\mathrm{di}} e^{-E_{3f}/(k_{\mathrm{B}}T)} \theta_2 (1-\theta_{\mathrm{tot}}) \\
\qquad\qquad - A_{\mathrm{as}} e^{-E_{3r}/(k_{\mathrm{B}}T)} \theta_3 \theta_{\mathrm{H}} - 2 \cdot A_{\mathrm{as}} e^{-E_{5f}/(k_{\mathrm{B}}T)} (\theta_{\mathrm{H}})^2, \\
\dfrac{d\theta_{\mathrm{ald}(g)}(t)}{dt} = A_{\mathrm{de}} e^{-E_{4f}/(k_{\mathrm{B}}T)} \theta_3.
\end{cases}
$$

Though the pre-exponential factors for the bond breaking processes may differ slightly, we assume the entropies of activation are approximately the same and near zero and assume 10^{13} s^{-1} for the dissociation pre-factor (A_{di}). The association pre-factor $A_{\mathrm{as}} = 10^{-2}$ cm^2/s was used for hydrogen recombination[62] and aldehyde hydrogenation reactions where all the reactants are mobile on the surface. $A_{\mathrm{as}} = 10^{-3}$ cm^2/s was used for alkoxide hydrogenation where the alkoxide is rigidly bound to the surface. Estimating that the density of surface active sites is about 1 site per 10 Å^2 surface area, equivalent to 10^{15} sites/cm^2, we converted the units of A_{as} to sites/s. The desorption pre-factors (A_{de}) of alcohols and aldehydes were estimated from the gas-phase entropies.[63] The activation energies (E_{if}, $i = 2, 3, 4$ and E_{jr}, $j = 1, 2, 3$) were adopted from the DFT-calculated kinetic barriers and binding energies (see values in Fig. 2 and Table 1). The barrier for hydrogen recombination to form H_2 ($E_{5f} = 0.60$ eV) was estimated from previous experimental measurement.[62] k_{B} is the Boltzmann constant, and T is the reaction temperature. To compare the dehydrogenation rates across different alcohols, the concentrations were all initiated as $\theta_{\mathrm{alc}(g)}(0) = \theta_1(0) =$

$\theta_3(0) = \theta_{\mathrm{H}}(0) = \theta_{\mathrm{ald}(g)}(0) = 0$ and $\theta_2(0) = 0.05$. We fixed the surface concentration of alkoxide $\theta_2(t)$ at 0.05, in order to fairly compare the catalytic capability of Cu(110) surface for the dehydrogenation of different alcohols by examining the varying production rates of aldehydes. The 0.05 monolayer coverage was chosen so that the $(1-\theta_{\mathrm{tot}})$ function has little effect on the model.

To solve the above ordinary differential equations, we used the Matlab ode23s solver which is based on an explicit Runge-Kutta formula.[64,65] We used a total simulation time t that was long enough for the surface species to reach steady state at reaction temperatures T of 500, 600, and 700 K. Fig. 6 shows the production rates of each aldehyde per surface area of Cu(110) at different T. Table 3 lists the steady-state concentrations of surface species and the production rates of alcohol(g) and aldehyde(g). The production of formaldehyde is quite slow. A high temperature is needed for speeding it up. The production efficiency of acetaldehyde is much larger than that of formaldehyde. The ratio of rates of production of acetaldehyde to formaldehyde is about 300 at 500 K, decreasing to about 200 and 100 at 600 K and 700 K, respectively. Overall, the simulated results here are reasonably consistent with the experimental observations of the lower production efficiency of formaldehyde[2,10,12,20] compared to acetaldehyde[16–19] on Cu. A high temperature is needed to produce anhydrous formaldehyde on Cu; however, an upper bound of temperature should exist to avoid its further decomposition into CO and H_2. The production rate of propionaldehyde is slightly higher than that of acetaldehyde. Due to its quite high desorption energy, the production rate of butyraldehyde is slower than those of acetaldehyde and propionaldehyde.

Since the β-hydride elimination step shows the highest activation barrier, we also studied the dependence of the production rate of formaldehyde on the kinetic pathway from $CH_3O(a)$ to $CH_2O{\cdot\cdot}H(a)$, which has an energy barrier of 0.93 eV (Fig. 2a). Among the initial, final, and transition states, we study the tuning of the energy levels of the transition (TS2) and final ($CH_2O{\cdot\cdot}H(a)$) states, because for the initial ($CH_3O(a)$) state there is strong covalent bonding between O and Cu and less room for adjusting its energy. We thus simulated the

formaldehyde production dependence on the two variables at $T = 500$ K - the energies of the transition state for C–H bond cleavage of the methoxy (TS2) and the energy of the dissociated state ($CH_2O{\cdot\cdot}H(a)$) (Fig. 7). In order to maximize the production rate a lower energy state is desired for both TS2 and the final state. Two main regions are found, separated at the curved positions of the black lines: in the upper left part where $E(\mathrm{TS2}) - E(CH_2O{\cdot\cdot}H(a))$ is smaller than about 0.35 eV, the rate depends strongly on the final-state energy and less on the transition-state energy, while at the bottom right corner the opposite is true. The original position of the production rate on Cu(110), marked as a star in the plot, is where *tuning the final-state energy is more effective*.

There are feasible approaches to reduce the energy levels of TS2 and $CH_2O{\cdot\cdot}H(a)$. For example, at the step edge sites of the pure Cu surface, or on the terrace of a Cu-based near-surface alloy,[20,66,67] the adsorption structure of methoxy can potentially be tuned so that the dissociating H becomes closer to its targeted adsorption site, and the hydrogen adsorption energy can be enhanced. By these avenues, the energies of TS2 and $CH_2O{\cdot\cdot}H(a)$ are generally expected to change by roughly the same amount. A dashed white line on Fig. 7 is added, along which the energy difference between the two states is fixed at 0.08 eV. Along this line, as the two energies decreases simultaneously, the production rate increases exponentially.

Our studies are focused on clean Cu(110), while the actual systems contain abundant defects and steps. These imperfect sites can potentially change the energetics and kinetics substantially, and in many cases they enhance the reactivity of the surface.[68] In future work, we plan to investigate how the kinetic pathway changes at the step and kink sites of Cu, especially the sites where Cu atoms have lower coordination. Additionally, Cu surfaces alloyed with other transition metals that have stronger bonding with H, e.g. Ni, Pd, and Pt,[69,70] will be examined to study their performance towards anhydrous formaldehyde production.

Before closing, it is important to note that the present study considers low coverages of surface intermediates. We ignore inter-molecule interactions by using a large supercell in the DFT calculations. In surface catalysis with reasonably high coverages of intermediates, the

stability of intermediates and reaction rates can depend on both the surface-molecule and molecule-molecule interactions.[41,71]

Conclusions

In summary, a comparative study of equilibrium structures and kinetic processes in the anhydrous dehydrogenation of methanol, ethanol, 1-propanol, and 1-butanol on the (110) surface of Cu, using multiscale approaches that combine first-principles calculations with vdW corrections and microkinetic rate analysis has been performed. Our studies clearly show the significance of vdW contributions to the adsorption of the reaction intermediates on the surface. We have detailed the kinetic pathways for anhydrous dehydrogenation for these alcohols, finding significant difference for methanol compared to the other alcohols. We simulated the production rates of aldehydes at a fixed alkoxide surface concentration, finding reasonable agreement with experimentally observed trends for methanol and ethanol dehydrogenation. In addition, we showed that increasing the reaction temperature and properly altering the rate-limiting process in methanol decomposition could provide more effective means of enhancing the production rate of anhydrous formaldehyde. We suggest that step or kink sites of pure Cu, and the terraces of Cu-based surface alloys are interesting structures for further investigation of their potential for more efficient methanol dehydrogenation. The present work not only provides insights into the different dehydrogenation behavior of linear-chain alcohols on Cu, but also sheds light on the cost-effective production of formaldehyde for industrial applications.

Acknowledgements

W.C. is grateful to Prof. Hannes Jónsson for helpful discussions. This work was supported by the Integrated Mesoscale Architectures for Sustainable Catalysis, an Energy Frontier Research Center funded by the U.S. Department of Energy, Office of Science, Basic Energy

Sciences under Award # DE-SC0012573. The calculations were performed at the the Oak Ridge Leadership Computing Facility (OLCF) and the National Energy Research Scientific Computing Center (NERSC) of the U.S. Department of Energy.

References

(1) Reuss, G.; Disteldorf, W.; Gamer, A. O.; Hilt, A. *Formaldehyde. Ullmann's Encyclopedia of Industrial Chemistry* **2000**,

(2) Wachs, I. E.; Madix, R. J. The selective oxidation of CH3OH to H2CO on a copper (110) catalyst. *J. Catal.* **1978**, *53*, 208–227.

(3) Pestryakov, A. N. Modification of silver catalysts for oxidation of methanol to formaldehyde. *Catal. Today* **1996**, *28*, 239–244.

(4) Dai, W.-L.; Liu, Q.; Cao, Y.; Deng, J.-F. Oxidative dehydrogenation of methanol to formaldehyde on electrolytic silver catalyst modified with iodides. *Appl. Catal., A: General* **1998**, *175*, 83–88.

(5) Nagy, A.; Mestl, G. High temperature partial oxidation reactions over silver catalysts. *Appl. Catal., A: General* **1999**, *188*, 337–353.

(6) Qian, M.; Liauw, M.; Emig, G. Formaldehyde synthesis from methanol over silver catalysts. *Appl. Catal., A: General* **2003**, *238*, 211–222.

(7) Waterhouse, G. I.; Bowmaker, G. A.; Metson, J. B. Mechanism and active sites for the partial oxidation of methanol to formaldehyde over an electrolytic silver catalyst. *Appl. Catal., A: General* **2004**, *265*, 85–101.

(8) Pestryakov, A. N.; Bogdanchikova, N.; Knop-Gericke, A. Alcohol selective oxidation over modified foam-silver catalysts. *Catal. Today* **2004**, *91*, 49–52.

(9) Su, S.; Prairie, M. R.; Renken, A. Promoting effect of active carbons on methanol dehydrogenation on sodium carbonate: hydrogen spillover. *Appl. Catal., A: General* **1993**, *95*, 131–142.

(10) Su, S.; Zaza, P.; Renken, A. Catalytic dehydrogenation of methanol to water-free formaldehyde. *Chem. Eng. Technol.* **1994**, *17*, 34–40.

(11) Musßicß, A.; Batista, J.; Levec, J. Gas-phase catalytic dehydrogenation of methanol to formaldehyde over ZnO/SiO 2 based catalysts, zeolites, and phosphates. *Appl. Catal., A: General* **1997**, *165*, 115–131.

(12) Dai, W.; Ren, L. *Dehydrogenation of Alcohols: Formaldehyde. Handbook of Heterogeneous Catalysis* **2008**,

(13) Lausche, A. C.; Hummelshøj, J. S.; Abild-Pedersen, F.; Studt, F.; Nørskov, J. K. Application of a new informatics tool in heterogeneous catalysis: analysis of methanol dehydrogenation on transition metal catalysts for the production of anhydrous formaldehyde. *J. Catal.* **2012**, *291*, 133–137.

(14) Lausche, A. C.; Abild-Pedersen, F.; Madix, R. J.; Nørskov, J. K.; Studt, F. Analysis of sulfur-induced selectivity changes for anhydrous methanol dehydrogenation on Ni (100) surfaces. *Surf. Sci.* **2013**, *613*, 58–62.

(15) Li, H.-J.; Lausche, A. C.; Peterson, A. A.; Hansen, H. A.; Studt, F.; Bligaard, T. Using microkinetic analysis to search for novel anhydrous formaldehyde production catalysts. *Surf. Sci.* **2015**, *641*, 105–111.

(16) Wachs, I. E.; Madix, R. J. The oxidation of ethanol on Cu (110) and Ag (110) catalysts. *Appl. Surf. Sci.* **1978**, *1*, 303–328.

(17) Eckert, M.; Fleischmann, G.; Jira, R.; Bolt, H. M.; Golka, K. *Acetaldehyde. Ullmann's Encyclopedia of Industrial Chemistry* **2000**,

(18) Chang, F.-W.; Yang, H.-C.; Roselin, L. S.; Kuo, W.-Y. Ethanol dehydrogenation over copper catalysts on rice husk ash prepared by ion exchange. *Appl. Catal., A: General* **2006**, *304*, 30–39.

(19) Sun, J.; Wang, Y. Recent advances in catalytic conversion of ethanol to chemicals. *ACS Catal.* **2014**, *4*, 1078–1090.

(20) Boucher, M. B.; Marcinkowski, M. D.; Liriano, M. L.; Murphy, C. J.; Lewis, E. A.; Jewell, A. D.; Mattera, M. F.; Kyriakou, G.; Flytzani-Stephanopoulos, M.; Sykes, E. C. H. Molecular-scale perspective of water-catalyzed methanol dehydrogenation to formaldehyde. *ACS Nano* **2013**, *7*, 6181–6187.

(21) Bowker, M.; Madix, R. XPS, UPS and thermal desorption studies of alcohol adsorption on Cu (110): I. Methanol. *Surf. Sci.* **1980**, *95*, 190–206.

(22) Russell, J.; Gates, S. M.; Yates, J. Reaction of methanol with Cu (111) and Cu (111)+ O (ads). *Surf. Sci.* **1985**, *163*, 516–540.

(23) Sexton, B. A. Surface vibrations of adsorbed intermediates in the reaction of alcohols with Cu (100). *Surf. Sci.* **1979**, *88*, 299–318.

(24) Sakong, S.; Gross, A. Total oxidation of methanol on Cu (110): a density functional theory study. *J. Phys. Chem. A* **2007**, *111*, 8814–8822.

(25) Mei, D.; Xu, L.; Henkelman, G. Potential energy surface of methanol decomposition on Cu (110). *J. Phys. Chem. C* **2009**, *113*, 4522–4537.

(26) Lorenzo, D. K.; Bradley, M. K.; Unterberger, W.; Duncan, D. A.; Lerotholi, T.; Robinson, J.; Woodruff, D. The structure of methoxy species on Cu (110): A combined photoelectron diffraction and density functional theory determination. *Surf. Sci.* **2011**, *605*, 193–205.

(27) Zuo, Z.-J.; Wang, L.; Han, P.-D.; Huang, W. Insights into the reaction mechanisms of methanol decomposition, methanol oxidation and steam reforming of methanol on Cu (111): A density functional theory study. *Int. J. Hydrogen Energy* **2014**, *39*, 1664–1679.

(28) García-Muelas, R.; Li, Q.; López, N. Density Functional Theory Comparison of Methanol Decomposition and Reverse Reactions on Metal Surfaces. *ACS Catal.* **2015**, *5*, 1027–1036.

(29) Ren, R.-P.; Zhang, Y.-C.; Liu, S.; Zuo, Z.-J.; Lv, Y.-K. DFT studies of the methanol decomposition mechanism on the H 2 O/Cu (110) and OH pre-adsorbed H 2 O/Cu (110) interfaces: Comparison with the clean Cu (110) surface. *Int. J. Hydrogen Energy* **2016**, *41*, 2411–2423.

(30) Wang, J.-H.; Lee, C.; Lin, M. Mechanism of ethanol reforming: theoretical foundations. *J. Phys. Chem. C* **2009**, *113*, 6681–6688.

(31) Li, R.; Zhang, M.; Yu, Y. A DFT study on the Cu (111) surface for ethyl acetate synthesis from ethanol dehydrogenation. *Appl. Surf. Sci.* **2012**, *258*, 6777–6784.

(32) Tereshchuk, P.; Da Silva, J. L. Ethanol and water adsorption on close-packed 3d, 4d, and 5d transition-metal surfaces: a density functional theory investigation with van der Waals correction. *J. Phys. Chem. C* **2012**, *116*, 24695–24705.

(33) Sun, K.; Zhang, M.; Wang, L. Effects of catalyst surface and hydrogen bond on ethanol dehydrogenation to ethoxy on Cu catalysts. *Chem. Phys. Lett.* **2013**, *585*, 89–94.

(34) Nørskov, J. K.; Abild-Pedersen, F.; Studt, F.; Bligaard, T. Density functional theory in surface chemistry and catalysis. *Proc. Natl. Acad. Sci. USA* **2011**, *108*, 937–943.

(35) Li, G.; Tamblyn, I.; Cooper, V. R.; Gao, H.-J.; Neaton, J. B. Molecular adsorption on metal surfaces with van der Waals density functionals. *Phys. Rev. B* **2012**, *85*, 121409.

(36) Ramalho, J. P. P.; Gomes, J. R.; Illas, F. Accounting for van der Waals interactions between adsorbates and surfaces in density functional theory based calculations: selected examples. *RSC Adv.* **2013**, *3*, 13085–13100.

(37) Studt, F.; Abild-Pedersen, F.; Varley, J. B.; Nørskov, J. K. CO and CO2 hydrogenation to methanol calculated using the BEEF-vdW functional. *Catal. Lett.* **2013**, *143*, 71–73.

(38) Liu, L.; Siegel, D. A.; Chen, W.; Liu, P.; Guo, J.; Duscher, G.; Zhao, C.; Wang, H.; Wang, W.; Bai, X. et al. Unusual role of epilayer–substrate interactions in determining orientational relations in van der Waals epitaxy. *Proc. Natl. Acad. Sci. USA* **2014**, *111*, 16670.

(39) Rodriguez-Reyes, J. C. F.; Siler, C. G.; Liu, W.; Tkatchenko, A.; Friend, C. M.; Madix, R. J. van der Waals interactions determine selectivity in catalysis by metallic gold. *J. Am. Chem. Soc.* **2014**, *136*, 13333–13340.

(40) Zhou, Y.; Chen, W.; Cui, P.; Zeng, J.; Lin, Z.; Kaxiras, E.; Zhang, Z. Enhancing the hydrogen activation reactivity of non-precious metal substrates via confined catalysis underneath graphene. *Nano Lett.* **2016**, *16*, 6058.

(41) Hiebel, F.; Shong, B.; Chen, W.; Madix, R. J.; Kaxiras, E.; Friend, C. M. Self-assembly of acetate adsorbates drives atomic rearrangement on the Au (110) surface. *Nat. Commun.* **2016**, *7*, 13139.

(42) Karakalos, S.; Xu, Y.; Kabeer, F. C.; Chen, W.; Rodríguez-Reyes, J. C. F.; Tkatchenko, A.; Kaxiras, E.; Madix, R. J.; Friend, C. M. Non-Covalent Bonding Controls Selectivity in Heterogeneous Catalysis: Coupling Reactions on Gold. *J. Am. Chem. Soc.* **2016**, *138*, 15243.

(43) Cheenicode Kabeer, F.; Chen, W.; Madix, R. J.; Friend, C. M.; Tkatchenko, A. First-Principles Study of Alkoxides Adsorbed on Au (111) and Au (110) Surfaces: Assessing

the Roles of Non-Covalent Interactions and Molecular Structures in Catalysis. *J. Phys. Chem. C* **2017**,

(44) Choi, J.-H.; Cui, P.; Chen, W.; Cho, J.-H.; Zhang, Z. Atomistic mechanisms of van der Waals epitaxy and property optimization of layered materials. *Wiley Interdiscip Rev Comput Mol Sci* **2017**, *7*.

(45) Kresse, G.; Furthmüller, J. Efficient iterative schemes for *ab initio* total-energy calculations using a plane-wave basis set. *Phys. Rev. B* **1996**, *54*, 11169–11186.

(46) Blöchl, P. E. Projector augmented-wave method. *Phys. Rev. B* **1994**, *50*, 17953–17979.

(47) Kresse, G.; Joubert, D. From ultrasoft pseudopotentials to the projector augmented-wave method. *Phys. Rev. B* **1999**, *59*, 1758–1775.

(48) Perdew, J. P.; Burke, K.; Ernzerhof, M. Generalized Gradient Approximation Made Simple. *Phys. Rev. Lett.* **1996**, *77*, 3865–3868.

(49) Tkatchenko, A.; Scheffler, M. Accurate Molecular Van Der Waals Interactions from Ground-State Electron Density and Free-Atom Reference Data. *Phys. Rev. Lett.* **2009**, *102*, 073005.

(50) Methfessel, M.; Paxton, A. T. High-precision sampling for Brillouin-zone integration in metals. *Phys. Rev. B* **1989**, *40*, 3616–3621.

(51) Henkelman, G.; Uberuaga, B. P.; Jónsson, H. A climbing image nudged elastic band method for finding saddle points and minimum energy paths. *J. Chem. Phys.* **2000**, *113*, 9901–9904.

(52) Henkelman, G.; Jónsson, H. A dimer method for finding saddle points on high dimensional potential surfaces using only first derivatives. *J. Chem. Phys.* **1999**, *111*, 7010–7022.

(53) Sakong, S.; Groß, A. Density functional theory study of the partial oxidation of methanol on copper surfaces. *J. Catal.* **2005**, *231*, 420–429.

(54) Dion, M.; Rydberg, H.; Schröder, E.; Langreth, D. C.; Lundqvist, B. I. Van der Waals Density Functional for General Geometries. *Phys. Rev. Lett.* **2004**, *92*, 246401.

(55) Lee, K.; Murray, E. D.; Kong, L.; Lundqvist, B. I.; Langreth, D. C. Higher-accuracy van der Waals density functional. *Phys. Rev. B* **2010**, *82*, 081101.

(56) Klimeš, J.; Bowler, D. R.; Michaelides, A. Van der Waals density functionals applied to solids. *Phys. Rev. B* **2011**, *83*, 195131.

(57) Xu, Y.; Chen, W.; Kaxiras, E.; Friend, C. M.; Madix, R. J. General Effect of van der Waals Interactions on the Stability of Alkoxy Intermediates on Metal Surfaces. *J. Phys. Chem. B* **2017**, *Article ASAP*.

(58) Madix, R.; Telford, S. Primary and secondary kinetic isotope effects for methoxy dehydrogenation and Cu (110): absence of tunnelling corrections. *Surf. Sci.* **1995**, *328*, L576.

(59) Chen, W.; Cui, P.; Zhu, W.; Kaxiras, E.; Gao, Y.; Zhang, Z. Atomistic mechanisms for bilayer growth of graphene on metal substrates. *Phys. Rev. B* **2015**, *91*, 045408.

(60) Dumesic, J. A. *The microkinetics of heterogeneous catalysis*; An American Chemical Society Publication, 1993.

(61) Davis, M. E.; Davis, R. J. *Fundamentals of chemical reaction engineering*; Courier Corporation, 2012.

(62) Anger, G.; Winkler, A.; Rendulic, K. Adsorption and desorption kinetics in the systems H2/Cu (111), H2/Cu (110) and H2/Cu (100). *Surf. Sci.* **1989**, *220*, 1–17.

(63) Campbell, C. T.; Árnadóttir, L.; Sellers, J. R. Kinetic prefactors of reactions on solid surfaces. *Z. Phys. Chem.* **2013**, *227*, 1435–1454.

(64) Dormand, J. R.; Prince, P. J. A family of embedded Runge-Kutta formulae. *J. Comp. Appl. Math.* **1980**, *6*, 19–26.

(65) Shampine, L. F.; Reichelt, M. W. The matlab ode suite. *SIAM J. Sci. Comput.* **1997**, *18*, 1–22.

(66) Greeley, J.; Mavrikakis, M. Alloy catalysts designed from first principles. *Nat. Mater.* **2004**, *3*, 810–815.

(67) Montemore, M. M.; Cubuk, E. D.; Klobas, J. E.; Schmid, M.; Madix, R. J.; Friend, C. M.; Kaxiras, E. Controlling O coverage and stability by alloying Au and Ag. *Phys. Chem. Chem. Phys.* **2016**, *18*, 26844–26853.

(68) Marcinkowski, M. D.; Murphy, C. J.; Liriano, M. L.; Wasio, N. A.; Lucci, F. R.; Sykes, E. C. H. Microscopic View of the Active Sites for Selective Dehydrogenation of Formic Acid on Cu (111). *ACS Catal.* **2015**, *5*, 7371–7378.

(69) Nørskov, J. K.; Bligaard, T.; Logadottir, A.; Kitchin, J.; Chen, J.; Pandelov, S.; Stimming, U. Trends in the exchange current for hydrogen evolution. *J. Electrochem. Soc.* **2005**, *152*, J23–J26.

(70) Chen, W.; Chen, H.; Lan, H.; Cui, P.; Schulze, T. P.; Zhu, W.; Zhang, Z. Suppression of grain boundaries in graphene growth on superstructured Mn-Cu (111) surface. *Phys. Rev. Lett.* **2012**, *109*, 265507.

(71) O'Connor, C. R.; Hiebel, F.; Chen, W.; Kaxiras, E.; Madix, R. J.; Friend, C. Identifying key descriptors in surface binding: Interplay of surface anchoring and intermolecular interactions for carboxylates on Au(110). *Chem. Sci.* **2018**,

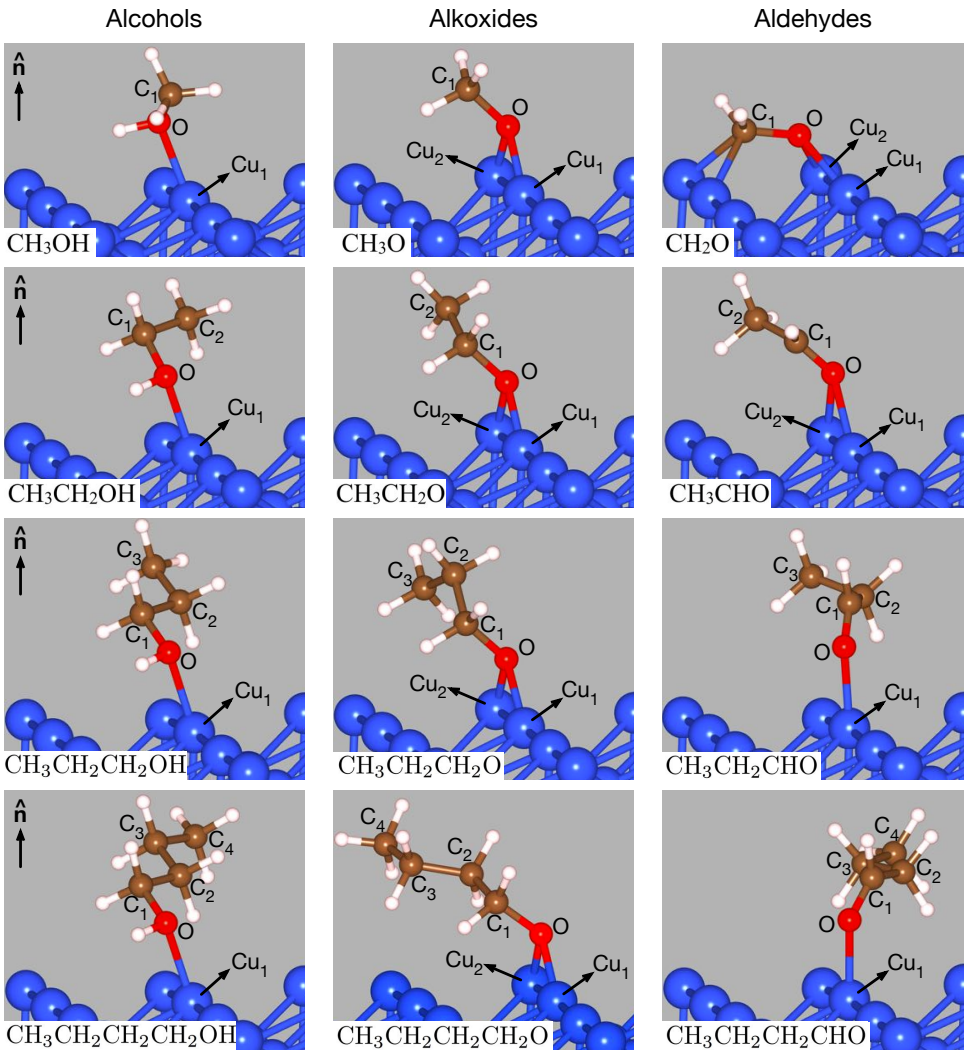

Figure 1: The most stable adsorption structures of reaction intermediates during methanol (1st row), ethanol (2nd row), 1-propanol (3rd row), and 1-butanol (4th row) dehydrogenation on Cu(110), calculated with vdW interactions included. $\hat{\mathbf{n}}$ is the surface normal vector. See their adsorption energies and structural parameters in Table 1.

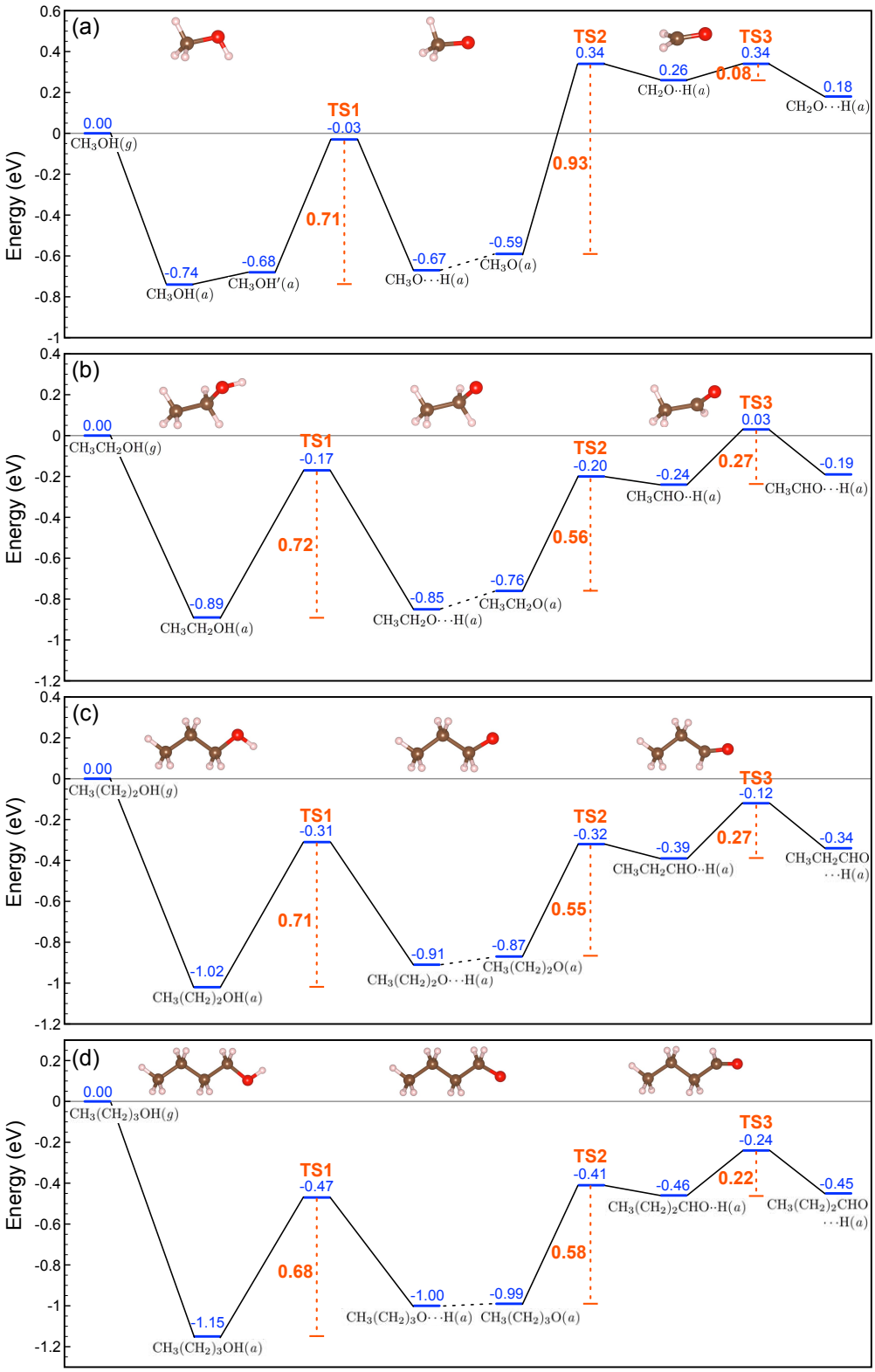

Figure 2: Potential energy paths of (a) methanol, (b) ethanol, (c) 1-propanol, and (d) 1-butanol dehydrogenation on Cu(110). In the formulas, (g) and (a) denote gas phase and adsorbed state, respectively. TS1, TS2, and TS3 are the transition states of O–H bond breaking, C–H bond breaking, and separation of H farther away from aldehyde, respectively.

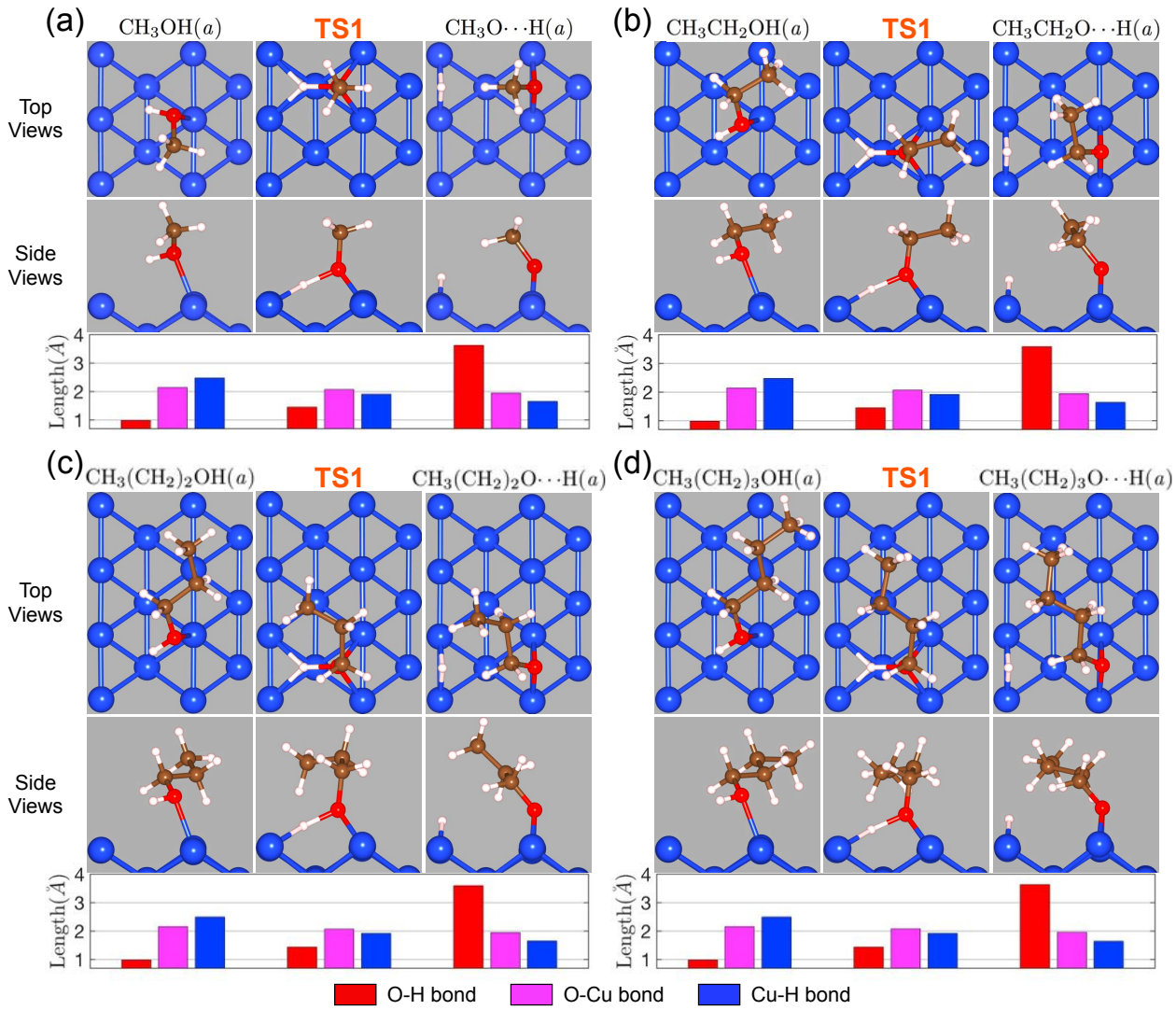

Figure 3: Structural configurations and parameters of the initial, transition, and final states in the O–H bond breaking of (a) methanol, (b) ethanol, (c) 1-propanol, and (d) 1-butanol, respectively. The formulas and symbols are consistent with those used in Figure 2. The dissociating H is used to measure the O–H and Cu–H distances. The shortest distances of O–Cu and Cu–H are chosen to show in the bar graphs, respectively.

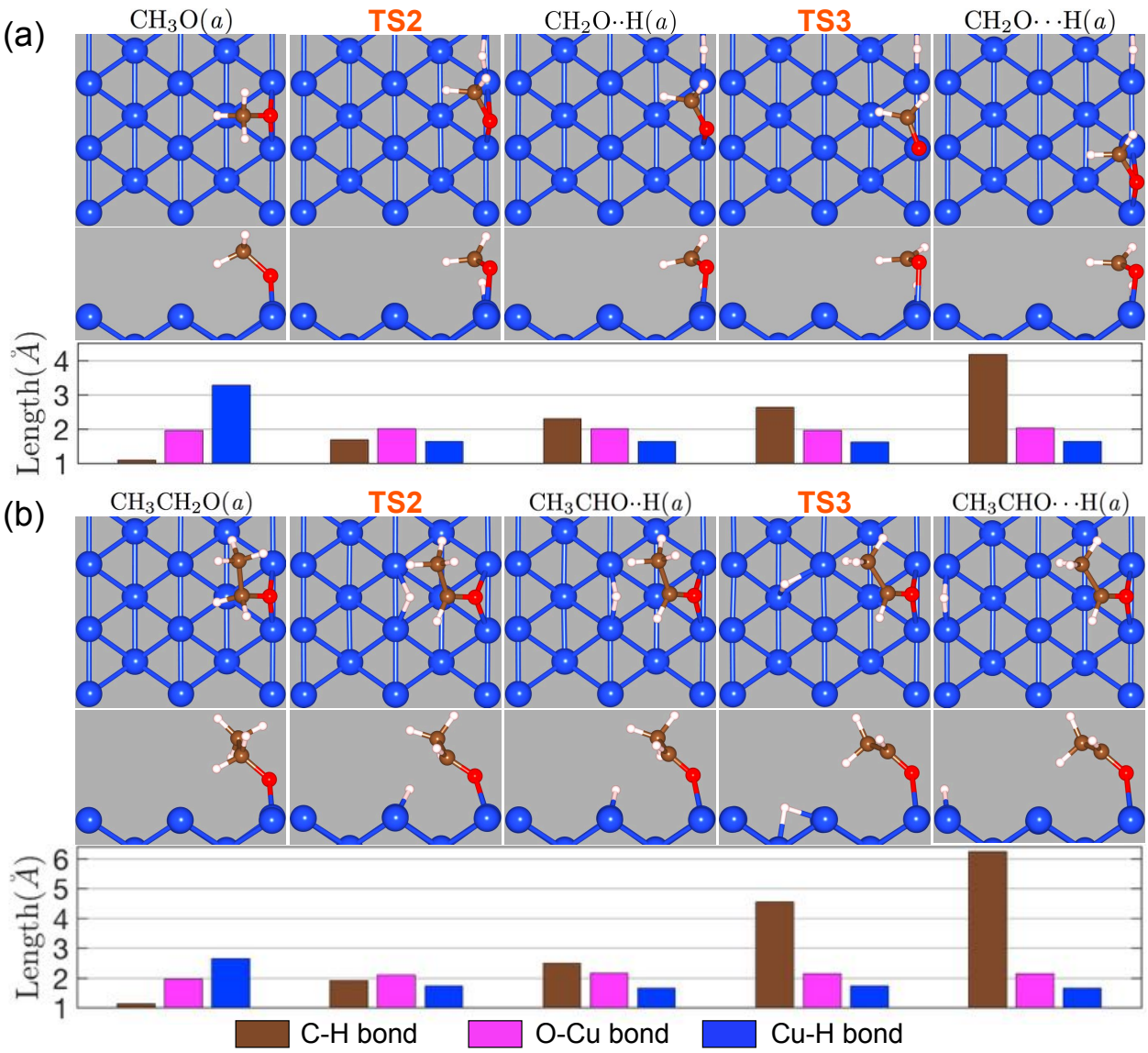

Figure 4: Structural configurations and parameters of the initial, transition, and final states in the C–H bond breaking (TS2) and the separation of H farther from the produced aldehyde (TS3) of (a) methoxy and (b) ethoxy. The dissociating H is used to measure the β-C–H and Cu–H distances. The shortest distances of O–Cu and Cu–H are chosen to show, respectively.

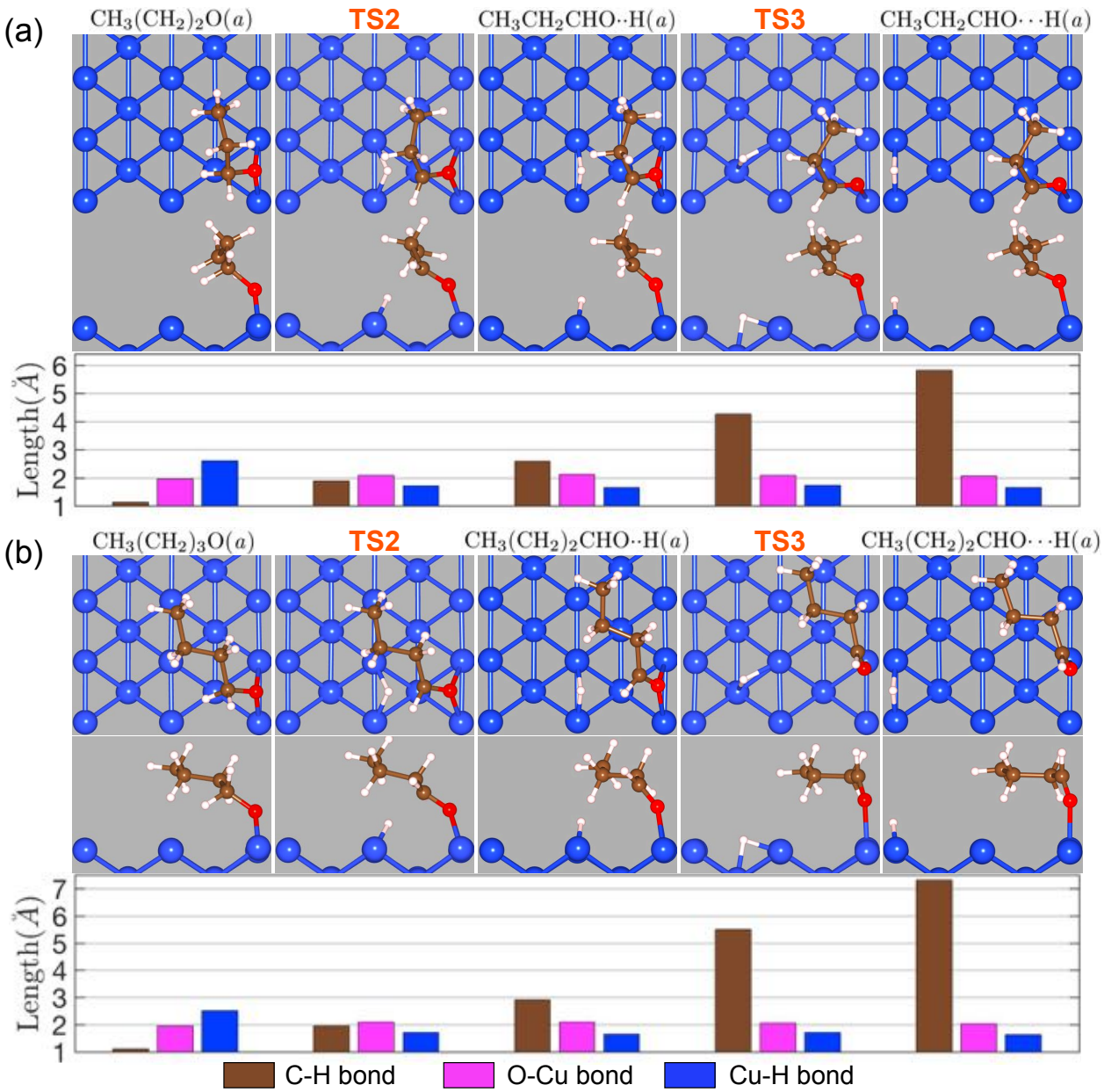

Figure 5: Structural configurations and parameters of the initial, transition, and final states in the C–H bond breaking (TS2) and the separation of H farther from the produced aldehyde (TS3) of (a) 1-propoxy and (b) 1-butoxy.

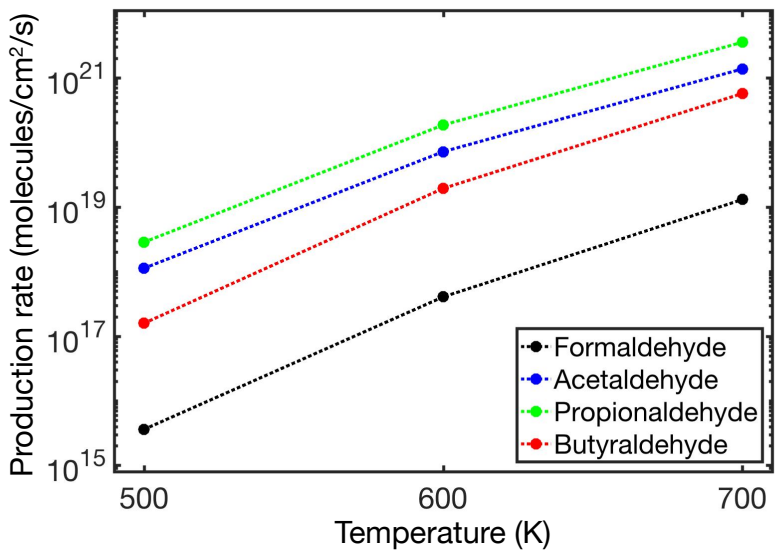

Figure 6: The simulated production rates per Cu(110) surface area (units: molecules/cm^2/s) of formaldehyde, acetaldehyde, propionaldehyde, and butyraldehyde from methanol, ethanol, 1-propanol, and 1-butanol decomposition, respectively, at different reaction temperatures.

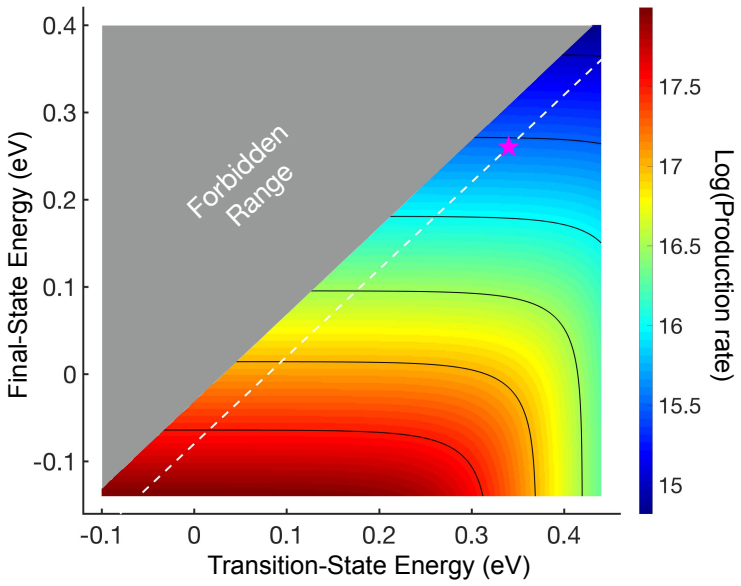

Figure 7: The dependence of production rate (unit: molecules/cm^2/s) of formaldehyde (on a log scale) on the energies of transition state (TS2, x-axis) and $CH_2O{\cdot\cdot}H(a)$ (y-axis), simulated at 500 K. The black lines are the equipotential lines, and the white dashed line shows the data with $E(\mathrm{TS2})-E(CH_2O{\cdot\cdot}H(a)) = 0.08$ eV. The magenta pentagram has x and y values obtained from the kinetic pathway in Fig. 2a. The forbidden range is where $E(\mathrm{TS2})-E(CH_2O{\cdot\cdot}H(a)) \leqslant 0.03$ eV.

Table 1: Adsorption energies ($E_{\mathbf{ads}}$) and structural parameters of reaction intermediates adsorbed on Cu(110) with and without vdW interactions. A more negative $E_{\mathbf{ads}}$ value means stronger adsorption.

Systems		E_{ads} (eV)		O-Cu bond length (Å)				$\angle(\overrightarrow{\mathbf{OC}_1}, \hat{\mathbf{n}})$	
				O-Cu$_1$ bond		O-Cu$_2$ bond			
		PBE	+vdW	PBE	+vdW	PBE	+vdW	PBE	+vdW
Alcohols	CH_3OH	−0.39	−0.74	2.15	2.14	–	–	48.0°	52.2°
	CH_3CH_2OH	−0.39	−0.89	2.16	2.14	–	–	49.8°	52.7°
	$CH_3(CH_2)_2OH$	−0.40	−1.02	2.16	2.16	–	–	54.6°	59.3°
	$CH_3(CH_2)_3OH$	−0.40	−1.15	2.17	2.16	–	–	55.6°	59.5°
Alkoxides	CH_3O	−2.50	−2.75	1.96	1.95	1.96	1.96	45.9°	47.9°
	CH_3CH_2O	−2.50	−2.89	1.96	1.96	1.96	1.96	44.4°	49.3°
	$CH_3(CH_2)_2O$	−2.50	−3.00	1.96	1.96	1.96	1.96	48.9°	50.4°
	$CH_3(CH_2)_3O$	−2.49	−3.12	1.97	1.96	1.97	1.98	51.6°	55.0°
Aldehydes	CH_2O	−0.47	−0.83	2.03	2.02	2.03	2.02	82.8°	84.0°
	CH_3CHO	−0.31	−0.79	2.42	2.23	2.15	2.15	41.1°	49.4°
	CH_3CH_2CHO	−0.34	−0.85	2.07	2.06	–	–	32.6°	38.8°
	$CH_3(CH_2)_2CHO$	−0.36	−1.06	2.06	2.04	–	–	34.2°	38.2°

Table 2: The elementary steps and their reaction rates used in the microkinetic analysis. θ_1, θ_2, θ_3, and $\theta_{\mathbf{H}}$ are the surface fractional coverages of alcohol(a), alkoxide(a), aldehyde(a), and H(a), respectively. The total surface coverage $\theta_{\mathbf{tot}}$ is equal to $\theta_1 + \theta_2 + \theta_3 + \theta_{\mathbf{H}}$. $A_{\mathbf{di}}$, $A_{\mathbf{as}}$, and $A_{\mathbf{de}}$ are the pre-exponential factors for the dissociation, association, and desorption reactions, respectively. E_{if} (i=2-5) and E_{jr} (j=1,2,3) are the activation energies. We did not take into account the adsorption processes of gas-phase alcohol and aldehyde and the dissociative adsorption process of H_2.

#	Elementary step	Forward rate	Reverse rate
1	alcohol(g) $\leftharpoonup$ alcohol(a)	–	$A_{\mathrm{de}}e^{-E_{1r}/(k_{\mathrm{B}}T)}\theta_1$
2	alcohol(a) $\rightleftharpoons$ alkoxide(a)+H(a)	$A_{\mathrm{di}}e^{-E_{2f}/(k_{\mathrm{B}}T)}\theta_1(1-\theta_{\mathrm{tot}})$	$A_{\mathrm{as}}e^{-E_{2r}/(k_{\mathrm{B}}T)}\theta_2\theta_{\mathrm{H}}$
3	alkoxide(a) $\rightleftharpoons$ aldehyde(a)+H(a)	$A_{\mathrm{di}}e^{-E_{3f}/(k_{\mathrm{B}}T)}\theta_2(1-\theta_{\mathrm{tot}})$	$A_{\mathrm{as}}e^{-E_{3r}/(k_{\mathrm{B}}T)}\theta_3\theta_{\mathrm{H}}$
4	aldehyde(a) $\rightharpoonup$ aldehyde(g)	$A_{\mathrm{de}}e^{-E_{4f}/(k_{\mathrm{B}}T)}\theta_3$	–
5	H(a)+H(a) $\rightharpoonup$ H_2(g)	$A_{\mathrm{as}}e^{-E_{5f}/(k_{\mathrm{B}}T)}(\theta_{\mathrm{H}})^2$	–

Table 3: The steady-state surface concentrations (units: monolayer coverage) of alcohols (θ_1), alkoxides (θ_2, fixed at 0.05), aldehydes (θ_3) and H ($\theta_{\mathbf{H}}$), and the desorption rates (units: monolayer/second) of alcohols ($d\theta_{\mathbf{alc}(g)}/dt$) and aldehydes ($d\theta_{\mathbf{ald}(g)}/dt$) from the surface at different temperatures (units: K).

	T	θ_1	θ_2	θ_3	θ_{H}	$d\theta_{\mathrm{alc}(g)}/dt$	$d\theta_{\mathrm{ald}(g)}/dt$
Methanol dehydrogenation	500	3.7E−8	0.05	7.2E−7	1.7E−4	3.1	3.6
	600	1.4E−7	0.05	3.2E−6	1.0E−3	2.1E+2	4.0E+2
	700	3.2E−7	0.05	1.0E−5	3.1E−3	3.8E+3	1.3E+4
Ethanol dehydrogenation	500	5.1E−6	0.05	3.5E−5	7.7E−3	5.2E+1	1.1E+3
	600	5.7E−6	0.05	1.0E−4	2.0E−2	1.9E+3	7.2E+4
	700	6.0E−6	0.05	2.1E−4	3.8E−2	2.3E+4	1.4E+6
1-Propanol dehydrogenation	500	2.1E−4	0.05	5.8E−5	1.1E−2	3.9E+2	2.9E+3
	600	1.3E−4	0.05	1.4E−4	3.1E−2	1.3E+4	1.9E+5
	700	8.3E−5	0.05	2.4E−4	6.0E−2	1.4E+5	3.5E+6
1-Butanol dehydrogenation	500	2.7E−4	0.05	1.1E−4	2.0E−3	8.9E+1	1.6E+2
	600	2.9E−4	0.05	2.1E−4	7.7E−3	8.4E+3	1.9E+4
	700	1.9E−4	0.05	3.3E−4	2.1E−2	1.4E+5	5.7E+5
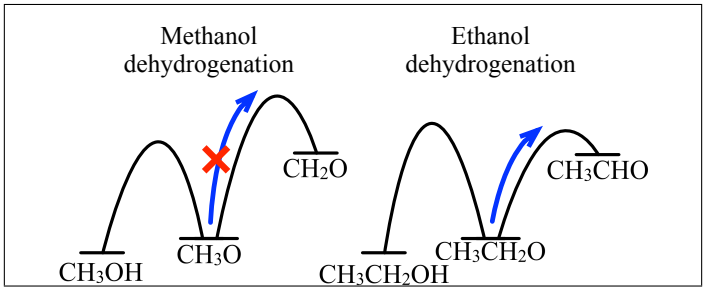
Graphical TOC Entry